INSTITUTE OF PHYSICS PUBLISHING JOURNAL OF MICROMECHANICS AND MICROENGINEERING

J. Micromech. Microeng. **16** (2006) S116–S124 doi:10.1088/0960-1317/16/6/S18

A micromachined capacitive incremental position sensor: part 1. Analysis and simulations

A A Kuijpers, G J M Krijnen, R J Wiegerink, T S J Lammerink and M Elwenspoek

Transducer Science & Technology Group, MESA+ Research Institute, University of Twente, The Netherlands

E-mail: a.a.Kuijpers@utwente.nl

Received 30 November 2005
Published 10 May 2006
Online at stacks.iop.org/JMM/16/S116

Abstract

Part 1 of this two-part paper describes the analysis and 2D finite element (FE) simulations for a capacitive incremental position sensor for nanopositioning of microactuator systems with a displacement range of 100 μm or more. Two related concepts for a capacitive incremental position sensor are presented. In an incremental capacitance measurement mode (ICMM), the periodic change in capacitance is measured to determine the relative displacement between two periodic geometries S1 and S2 with a gap distance of $\sim$1 μm. In a constant capacitance measurement mode (CCMM), the distance between S1 and S2 is controlled to keep the capacitance between S1 and S2 constant. Analysis and 2D finite element simulations show that the signal-to-noise ratio for CCMM can be $>300\times$ over ICMM and with less nonlinearity of the position sensor signal. This means that CCMM will perform better in accurate quadrature incremental position detection. A comparison with measurements shows that the 2D finite element simulation method is a useful tool that realistically predicts the capacitance versus displacement for different combinations of periodic geometries.

(Some figures in this article are in colour only in the electronic version)

1. Introduction

This is part 1 of a two-part paper and it presents a theoretical and numerical analysis for a capacitive long-range position sensor for nanopositioning of microactuator systems. In part 2, the microfabrication and experimental assessment are presented.

1.1. Long-range position sensing and control in MEMS applications

Provided that nanometer position accuracy can be obtained over tens of μm displacement range, microactuators have a high potential in future probe memory applications [1, 2], scanning probe microscopy [3–5], medical analysis [6], cell manipulation (e.g. DNA analysis [7], neuron analysis in neurophysiology [8], microbiology applications [9]), optical applications (e.g. mirror manipulation) [10] and microtooling and robotics (e.g. microgripper) [11].

For these applications that require high-precision displacements over a long range, which may not be obtained using open-loop operation, a combination of position sensing and control is necessary. In general, with the addition of position control, the performance of a system can be improved and the sensitivity to parameter variations and external disturbances (e.g. noise, vibrations) can be reduced. To enable position control with nanometer accuracy over 100 μm displacement (or more), a position sensor is required with a (very) high ratio of displacement over resolution, i.e. dynamic range.

Typically, the performance of these MEMS-based devices will increase if the position sensor is fully integrated with the

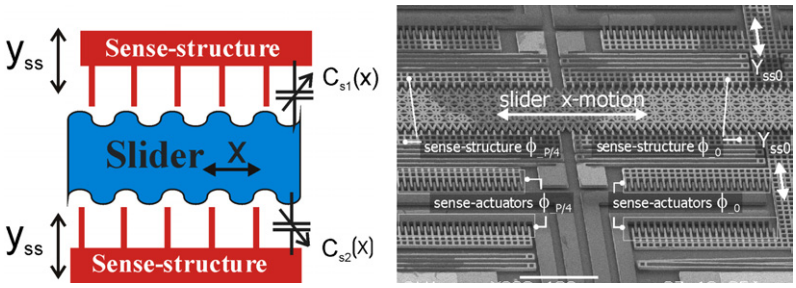

Figure 1. Left: the capacitive incremental position sensor in concept. Right: example of a micromachined test device with an integrated sensor.

device in combination with position control. In order to make such systems both economically viable and compact, on-chip position sensing appears to be a requirement. Commonly, this means the hybrid integration of the MEMS part and the sensing electronics (e.g. CMOS), which is sometimes simpler and economically more feasible [12].

Recently, Pantazi *et al* have reported on a servo-tracking control mechanism for the Millipede project. A media sled or storage medium scanner is positioned with x/y motion range capabilities on the order of 120 μm [1, 13, 14]. The experimental results reported by Pantazi show the feasibility of closed-loop track following using thermal position sensor signals yielding a position-error standard deviation of approximately 2 nm over a range of ± 10.1 μm. The fabrication of the complete system is not fully micromachined but involves microassembly of the inductive microcoil x/y-actuators to the medium.

Chu and Gianchandani [15] report on a 2D positioner with electrothermal actuation and sub-nanometer capacitive sensing. The displacement of the actuator is amplified by a mechanical amplifier and measured using a comb-structure. The construction allows the structure to achieve 19 μm displacement at sub-nanometer resolution, but with a significant uncertainty in the lever design and the characterization method.

In the two references quoted above, a position sensor with a non-periodic sensor signal is used, i.e. a non-incremental sensing principle is applied. However, eventually at some maximum range of displacement it will become increasingly difficult to obtain nanometer precision with a non-incremental principle, due to limitations in signal-to-noise ratio (SNR), nonlinearity and stability.

1.2. Incremental position sensing

This paper presents and describes a capacitive incremental position sensing principle, which is based on a periodic sensor signal. In the field of measurement and instrumentation, the concept of an incremental position sensor is commonly used with optical interferometers, incremental optical and capacitive encoders, rotary shaft encoders and resolvers [16–20]. It is the solution for the combination of a desired very high dynamic range and high accuracy. Two periodic sensor signals $s_1(x)$ and $s_2(x)$ with a mechanical offset of a quarter period $(P/4)$ between the two are necessary to unambiguously determine the position within each period [16, 21]. Ideally, these signals are pure sine and cosine or perfect triangular shaped. Coarse position detection is established by detecting the half periods of each signal with an up–down counter, and discrete increments of a quarter period can be counted. This principle is called quadrature detection because it divides a period into four quadrants and forms the easiest way to measure a certain displacement [16].

More precise position detection combines the coarse position detection with a fine analog/interpolation measurement of the position using an arctan calculation or a look-up table. The displacement can be detected with an accuracy limited by noise, nonlinearity and stability [16].

The novel capacitive incremental position sensor reported here is based on two related concepts (described in section 2).

- Incremental capacitance measurement mode ICMM (open-loop)
- Constant capacitance measurement mode CCMM (closed-loop)

Earlier, in advance of microfabrication of devices to perform experiments with, we reported on 2D FE simulations for both concepts to conclude that capacitance changes versus displacement could be expected to be measurable [22]. Results from the first quasi-static experiments with micromachined devices were reported earlier in [23, 24]. With these results, we have demonstrated that the concepts are realizable and could lead to a long-range position microsensor with nanometer accuracy. Specifically, for CCMM, a better performance is suggested by the results reported so far.

In this paper we present a theoretical estimation of the increase in signal-to-noise ratio and improvement in nonlinearity for CCMM. A comparison between actual measurements and 2D FE simulations for ICMM is presented to determine if the 2D FE simulation method realistically predicts the capacitance versus displacement for different combinations of periodic geometries. The conclusion on this new comparison justifies the use of the 2D FE method in section 4 to examine the difference in performance between ICMM and CCMM in terms of nonlinearity. In part 2 of this paper, the microfabrication and experimental assessment are presented. A complete overview of this research project and the results can be found in [25].

2. Capacitive incremental position sensor

The two concepts ICMM and CCMM are based on the change in capacitance between two periodic geometries for a relative displacement between the two as depicted in figure 1. Both

slider and sense-structures have opposing periodic patterns. It is the position (x) of the slider that has to be measured by measuring the change in capacitance $\Delta C_s(x)$. The aim is to integrate this position sensing principle with a micromachined microactuator to improve the performance at a limited cost. Figure 1 (right) gives an example of a capacitive incremental position sensor, made by surface micromachining of a 5 μm thick boron-doped poly-silicon layer. The structure is released with a freeze-drying process after etching the sacrificial oxide layer underneath the poly-layer. More details of the fabrication are given in part 2.

2.1. Incremental capacitance measurement mode

In incremental capacitance measurement mode (open-loop), the capacitance between the slider and sense-structure changes periodically as the slider beam moves (x-direction). Two pairs of sense-structures with a quarter period shift will produce two periodic signals, which are used for quadrature incremental position sensing of the slider. Additional sense-actuators (comb-drives) are used to reduce the design gap between the slider and sense-structure and thus increase the capacitance $C_s(x)$ and capacitance variation $\Delta C_s(x)$. The active gap reduction is done only once before the actual measurement operation starts. This way the gap can be made smaller than the minimum resolvable distance of $\sim$2 μm in the mask design which is limited by the standard available photo-lithography of the Mesa$^+$ laboratory.

2.2. Constant capacitance measurement mode

In constant capacitance measurement mode, the sense-actuators are closed-loop controlled in order to keep the capacitance C_s constant, equal to a setpoint value C_{setpoint} (i.e. $C_s = C_0$, $\Delta C_s = 0$). As a result of the motion of the slider in the x-direction, the sense-structures will move in the y-direction, closely following the pattern on the slider. The required sense-actuator voltage (i.e. the control voltage $U_c(x)$) will become periodic and a measure for the slider displacement. This method is expected to give a better signal-to-noise ratio, because for all positions within a period, the sensor capacitance is kept at a larger constant value than is possible with open-loop operation.

2.3. Estimation of SNR for ICMM and CCMM

This section gives a derivation to estimate the increase in the SNR for the CCMM concept over the ICMM concept, see figure 2.

- In the ICMM concept, the capacitance between geometries S1 and S2 changes periodically for a relative displacement (x) between S1 and S2.
- In the CCMM concept, the periodic geometry S2 is displaced in the y-direction for every x-position to keep the capacitance $C(x, y)$ equal to a setpoint value, i.e. $C(x, y(x)) = C_{\text{setpoint}}$.

In practice, the situation given in figure 2 will be in between the two extremes depicted in figure 3. As a first-order approximation, for the probe-like geometry in figure 3, the ratio of the width of the tip (3D) or plate (2D) to the distance $d(x)$ between the probe and plate is infinitely small ($w/d \to 0$), the field intensity will be mostly non-uniform and concentrated between the tip and the bottom surface area (plate) and the shape of the probe, rounded or rectangular, is no longer important. If the fingers in figure 3 have a certain limited width, then continuously decreasing the gap d will end up with a situation depicted by the parallel plate-like geometry in figure 3. The field intensity will be mostly uniform and concentrated between the top plate and bottom plate. Here, the average width d_{mean} is important if the top or bottom surface is curved or at an angle.

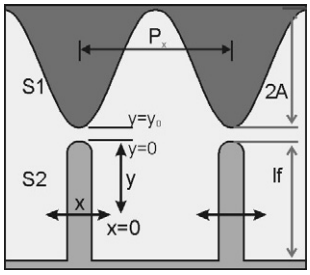

Figure 2. Geometry combination to derive an estimate of the SNR for ICMM and CCMM.

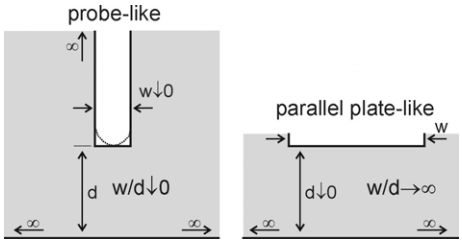

Figure 3. A probe-like capacitance and a parallel plate-like capacitance; two basic capacitance models are considered as two extreme situations, the model for figure 2 somewhere in between.

So the assumption of probe-like dimensions in figure 2 means that, for ICMM, the ratio of the period size P_x over the width of the fingers w is large (i.e. $\alpha = P_x/w >> 1$) and, for CCMM, an additional assumption is that finger length ℓ_f is much larger than the amplitude of geometry S1, i.e. $\ell_f \gg 2A$.

For position detection, only the change in capacitance ΔC versus displacement (x) is relevant, assuming constant parasitic capacitance C_p. In ICMM (open-loop), the change in capacitance between geometries S1 and S2 with probe-like dimension ratios is reasonably approximated by

$$\Delta C(x) = \frac{C_0}{y_0 + A(1 - \cos kx)}. \tag{1}$$

The term C_0 (in F m) includes the structure height h, and $k = 2\pi/P_x$ (in μm^{-1}). The SNR$_c$ for ICMM is defined by the amplitude of ΔC divided by the noise contribution δC, and is given by

$$S/N_c = \frac{\Delta\hat{C}}{\delta C} = \left[\frac{C_0 \cdot A}{y_0 \cdot (y_0 + 2A)}\right] \cdot \frac{1}{\delta C}. \tag{2}$$

In CCMM, geometry S2 is moveable in the y-direction by an additional comb-drive actuator. For a comb-drive actuator, the displacement y is proportional to the square of the applied

voltage U. Reducing the gap between S1 and S2 will increase the capacitance. The capacitance between S1 and S2 becomes

$$C(x, U_c) = C_p + \frac{C_0}{y_0 + A(1 - \cos kx) - KU_c^2}, \tag{3}$$

with C_0 in F m and K in m V^{-2}.

For position detection, the change in control voltage ΔU_c ($C_{setpoint}$, x) is used, which is the difference between $U_c(x)$ and $U_{setpoint}$. For an arbitrary position $0 < x < P_x$, the voltage U_c is such that $C(x, U_c) = C_{setpoint}$. Thus, we can write for the voltage U_c:

$$U_c^2 = \frac{1}{K}\left[y_0 + A(1 - \cos kx) - \left[\frac{C_{setpoint} - C_p}{C_0}\right]^{-1}\right]. \tag{4}$$

Neglecting a term ΔU_c^2 in the derivation, the expression for the change in voltage $\Delta U_c(x)$ versus displacement (x) becomes

$$\begin{aligned} U_c^2 - U_{setpoint}^2 &\approx 2 \cdot \Delta U_c(x) \cdot U_{setpoint} = \frac{1}{K}[-A\cos kx] \\ \Delta U_c(x) &= \frac{1}{2KU_{setpoint}}[-A\cos kx]. \end{aligned} \tag{5}$$

At position $x = P_x/4$, the voltage $U_c = U_{setpoint}$ for which the capacitance $C(P_x/4, U_{setpoint}) = C_{setpoint}$. A disturbance of the capacitance with δC due to noise or changes in humidity or temperature will lead to a change in the voltage ΔU_c with δu to compensate the change δC,

$$\begin{aligned} U_c^2 &= (U_{setpoint} + \Delta U_c(x) + \delta u)^2 \\ &= \frac{1}{K}\left[y_0 + A(1 - \cos kx) - \left[\frac{C_{setpoint} - C_p - \delta C}{C_0}\right]^{-1}\right]. \end{aligned} \tag{6}$$

Using $U_c^2 = (\Delta U_c(x) + \delta u)^2 \ll 2 \cdot (\Delta U_c(x) + \delta u) \cdot U_{setpoint}$, the expression for the SNR for CCMM becomes (SNR$_u$)

$$S/N_u = \frac{\Delta \hat{U}_c(x)}{\delta u_c} = \frac{A}{\left(y_0 + A - KU_{setpoint}^2\right)^2} \cdot \frac{C_0}{\delta C}. \tag{7}$$

The estimation of the improvement in the SNR for CCMM in comparison with ICMM is determined by the ratio SNR$_u$/SNR$_c$:

$$\frac{S/N_u}{S/N_c} = \frac{y_0 \cdot (y_0 + 2A)}{\left(y_0 + A - KU_{setpoint}^2\right)^2}. \tag{8}$$

For amplitude $A = 4$ μm, $y_0 = 2$ μm, and a controlled gap between geometries S1 and S2 of $g = y_0 + A - K \cdot U_{setpoint}^2 = 0.25$ μm, gives an improvement of SNR$_u$ of ~320× SNR$_c$ for CCMM over ICMM.

The following conclusions are drawn.

- From the expression in equation (8), it is concluded that the SNR for CCMM increases when
  (1) the amplitude A of the periodic geometry S1 is large and the term C_0 which includes the structure height h is also large, and
  (2) $KU_{setpoint}^2 \sim y_0 + A$, i.e. small gap size,
- The shape of geometry S1 is recovered well in the control voltage $U_c(x)$ and, ideally, geometry S1 would be pure sine or triangular shaped as described by equation (5).

Table 1. The design parameters of the different geometries included in the simulations and measurements.

Name	Period (μm)	Designed gap distance g_d
Rect-RectP8 (RectP8)	8	2
Rect-RectP12 (RectP12)	12	1.5
Sin-RectP10 (SinP10)	10	1.5
Sin-RectP16 (SinP16)	16	1
Trian-RectP16 (1 × TrianP16)	16	1
Trian-TrianP16 (2 × TrianP16)	16	0.5

3. A comparison of 2D FE simulations with measurements for a micromachined capacitive incremental position sensor

This section gives a comparison between 2D FE simulations and measurements for a micromachined capacitive incremental position sensor. The actual capacitance measurement method and results are described in full detail in part 2 of this paper.

The first objective is to prove that the concept of a periodically changing capacitance can be realized and to demonstrate the influence of different geometries on the shape of the output function in relation to the displacement of the slider, for both simulations and measurements. The second objective is to examine how well the 2D FE simulations, as an alternative to the computationally more time-consuming 3D FE simulations, predict the shape and the absolute value of the capacitance function $\Delta C(x)$. The simulation method described in [24] has been further developed and automated using a Matlab script file for FEMLAB software [26]. The conclusion on this new comparison justifies the use of the 2D FE method in section 4 to further examine the difference in performance between ICMM and CCMM in terms of nonlinearity.

First, we will demonstrate that each geometry produces a measurable output function and has distinguishable shape characteristics, i.e. the SNR for the experimental setup is sufficient to detect different shape and amplitude characteristics. At this stage, the aim is not to compare each selected measured capacitance function for each geometry with a pure sine or triangular function and quantify the resemblance.

In figure 4 and table 1, different geometries and their naming are given. And, as an example, a photograph is given of a realized device with a sine–rectangular geometry combination on the slider and sense-structures with a period of 10 μm (SinP10). The photograph in figure 4 (right) shows that the fabrication technology (plasma-etching) has rounded the 'fingers' and other features. The design name is based on rectangular fingers, but in practice the fingers turn out to have rounded edges.

An important parameter is the designed gap distance g_d indicated in table 1. It is the minimum gap distance as drawn in the mask design. The resolution of the available standard lithography is limited to roughly 2 μm.

For the particular measurements discussed here, the devices did not have the possibility to electronically control the gap size between the sense-structures and slider with additional comb-drive actuators.

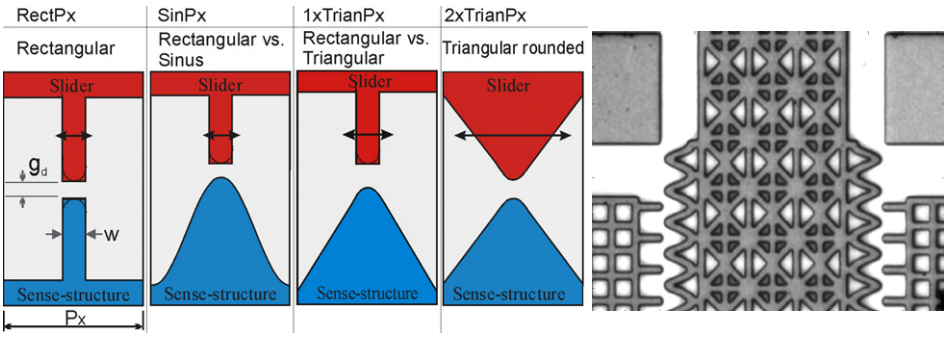

Figure 4. Left: the naming of the different geometries used in the simulations and measurements. Right: an example of a realized device showing a sine versus rectangular geometry with a period of $P_x = 10\ \mu$m, i.e. SinP10.

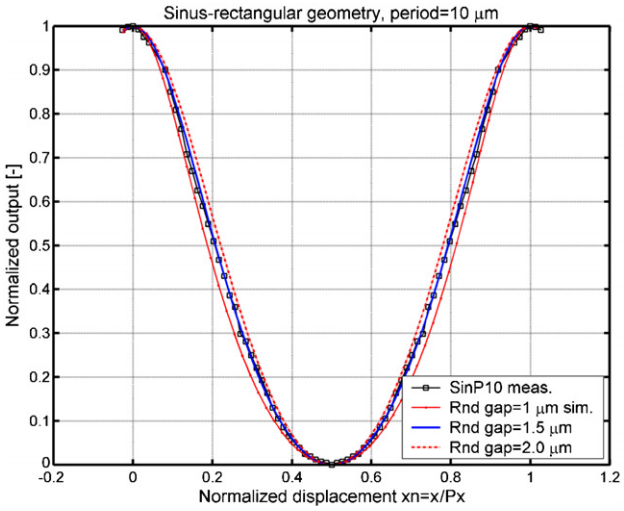

Figure 5. The SinP10 combination, the normalized measured curve and three simulated curves. Simulations for rounded instead of rectangular fingers show a very good fit for a gap distance g equal to the designed gap distance g_d.

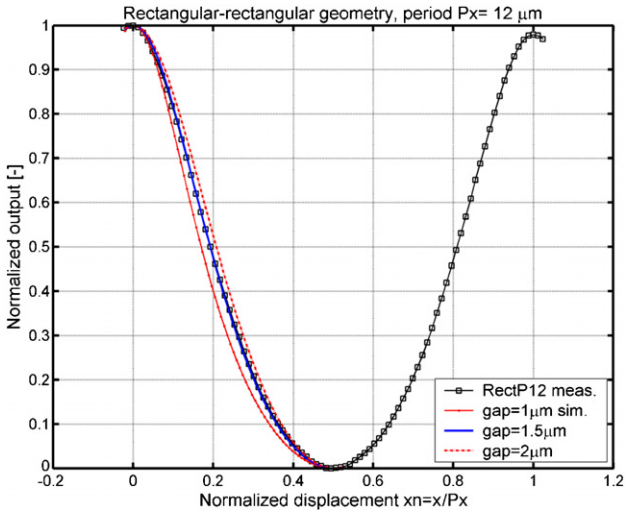

Figure 6. The normalized measured curve and three simulated curves for the RectP12 combination. A perfect fit is found for simulation with a gap $g = 1.5\ \mu$m.

A change in capacitance results in a change in output voltage of the measurement electronics. The simulated and measured capacitance functions are normalized in amplitude and displacement to be compared in terms of shape, i.e. $C_n = (C_{out}(x) - (C_{out})_{min})/(\Delta C)_{max}$ and $x_n = x/P_x$.

3.1. A qualitative comparison between 2D FE simulations and measurements of ICMM

In figure 5 a comparison is given between the normalized measured curve and three simulated curves for a geometry combination of rectangular fingers on the sense-structures and a sine pattern on the slider. The period $P_x = 10\ \mu$m (SinP10) and the designed gap distance $g_d = 1.5\ \mu$m. The simulated curves are for fingers with rounded edges as indicated in figure 4, and the minimum gap distances are respectively $g = 1\ \mu$m, $g = g_d$ (i.e. $=1.5\ \mu$m) and $g = 2\ \mu$m. It is clear from figure 5 that a gap distance close or equal to the designed gap distance of $g_d = 1.5\ \mu$m will give a simulation result corresponding very well to the normalized measured curve.

Figure 6 gives the normalized measured curve and three simulated curves for the RectP12 combination. A perfect fit is found for simulation with a gap g equal to the designed gap distance $g_d = 1.5\ \mu$m.

The conclusion is that the simulation with the 2D finite element method with the assumption of infinitely high geometries as described in [24] is indeed a useful tool to realistically predict the shape of the capacitance versus displacement for different combinations of geometries. The absolute capacitance value may differ considerably from the value encountered in a realized micromachined sensor due to the unknown addition of parasitic capacitance. This is examined in the following section.

3.2. A quantitative comparison between simulated and measured capacitance functions of ICMM

The output voltage of the measurement electronics is calibrated with the use of fixed discrete capacitor components. With the acquired linear relations, the measured capacitance functions (in voltage) for different micromachined geometries are converted to units of capacitance (F) and compared in figure 7 with 2D FE simulated curves. Naturally, 2D FE simulations do not simulate the 3D effects of a ground plane underneath the structure, or the additional parasitic capacitance C_p. However, under the assumption that the correspondence between the

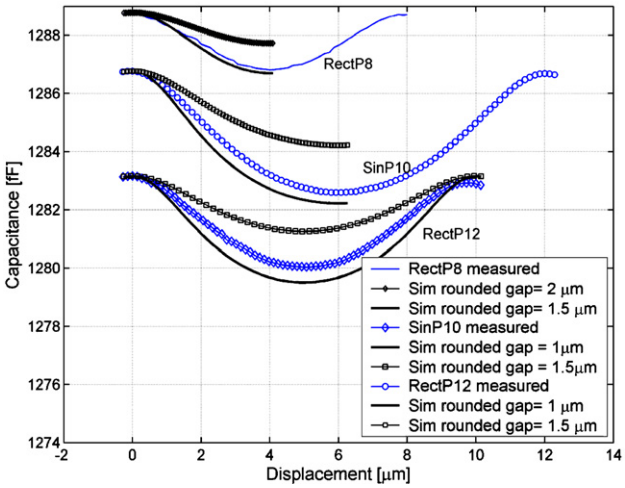

Figure 7. A comparison between measured and simulated capacitance functions.

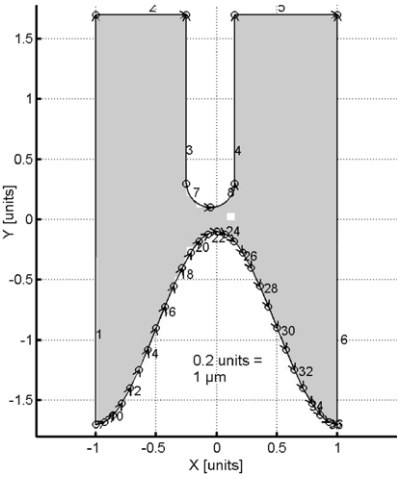

Figure 8. Geometry for 2D FE simulations, the geometry combination sine–rounded finger and period $P_x = 10\ \mu$m (=2 units).

measured and simulated capacitance functions will be best at the maximum capacitance when the gap between the two geometries (S1 and S2) is minimal, the simulated graphs are vertically aligned by making the simulated maximum value equal to the measured maximum value.

The comparison for three geometry combinations given in figure 7 shows that for the simulated curves with a gap g smaller than the designed gap distance g_d as indicated in figure 4 and table 1, the correspondence is better.

With the gap $g = g_d$, the simulated maximum change $(\Delta C_{sim})_{max}$ is smaller than the measured maximum change $(\Delta C_{meas})_{max}$.

One obvious possible cause for this effect is the deviation between feature sizes of fingers and gaps in the mask design and the realized feature sizes after processing (i.e. lithography and plasma etching). A deviation of 100–200 nm is not unrealistic.

Another possible cause for the fact that $(\Delta C_{sim})_{max} < (\Delta C_{meas})_{max}$, if $g = g_d$, may be the 3D effect of straying capacitance caused by the ground plane underneath the structures.

Applying a voltage V to two electrodes generates an amount of charge Q on the electrodes and a total flux Ψ between the two electrodes, emanating from one electrode and terminating on the other. The capacitance C between the two electrodes is defined by the total flux Ψ or the amount of charge Q that is produced by applying a voltage V:

$$\Psi = Q = C \cdot V. \tag{9}$$

For a two-electrode system, all flux lines which emanate on one electrode will terminate on the other and directly contribute to the capacitance. For a multiple-electrode system, this is generally not true [16].

For a half-period displacement ($x = P_x/2$), when the distance between the geometries is the largest, the ground plane will have the most influence, and the measured capacitance between the two geometries may be smaller than that predicted by 2D simulations. Field flux lines will originate on the charges on one geometry and terminate directly on the opposite charges on the surface of the substrate. Therefore, the number of field lines or the amount of flux directly linking the two geometries will be smaller than without the ground plane, and thus the capacitance between the two geometries will be smaller with the ground plane (e.g. described in [16, 27]).

4. Nonlinearity study for ICMM and CCMM using 2D FE simulations

The analysis in section 2.3 predicts a better performance for the CCMM concept in terms of nonlinearity and in particular a sinusoidal function $y(x)$ if a geometry combination of a sine on the slider and sense-fingers with probe-like dimensions is chosen. In this section, this prediction is examined through new 2D FE simulations and a Fourier analysis for both ICMM and CCMM.

4.1. Nonlinearity study for ICMM

For the geometry given in figure 8, the resulting capacitance functions for ICMM for two gap sizes $g_1 = 0.5\ \mu$m and $g_2 = 0.2\ \mu$m, corresponding to a maximum capacitance of $C_1 = 200$ aF and $C_2 = 300$ aF, are given in figure 9. This is the capacitance per finger-pair segment for a structure height of 5 μm [24]. Again, it is noted that because of the scaling properties of the 2D Laplace equation, these position-sensing principles can also be used in macro-scale applications as well.

The first harmonic in the space domain is $f_1(x) = C_{\omega 0}(x) = A_{\omega 0} \cdot \cos(\omega_0 \cdot x)$. A residual function $r(x)$ is defined as the difference in the space domain between the function $f(x)$ and the first harmonic $f_1(x)$, i.e. $r(x) = f(x) - f_1(x)$. In other words, this is the nonlinearity due to higher-order harmonics. The average amplitude $r(x)$ is defined as $\overline{r(x_n)} = (\max(r(x_n)) - \min(r(x_n)))/2$.

With the inverse FFT for all residual higher-order frequency components of the capacitance functions $C(x)$, the amplitude of the function $r(x)$ is determined. The ratio with the amplitude $A_{\omega 0}$ of the first-order harmonic $f_1(x)$ is given in table 2.

For a smaller gap $g_2 = 200$ nm corresponding to a maximum capacitance $C_2 = 300$ aF, the contribution of the

Table 2. ICMM amplitudes and ratios for the FFT components of simulated $C(x)$ for different gaps g.

g (nm)/C (aF)	$A_{\omega 0}$ (aF) $_{(\omega 0=0.2\pi)}$	$A_{2\omega 0}/A_{\omega 0}$	$A_{3\omega 0}/A_{\omega 0}(x)$	$\overline{r(x_n)}$ (aF)	$\overline{r(x_n)}/A_{\omega 0}$
500/200	36.9136	0.3012	0.0975	13.3589	0.3619
200/300	72.1783	0.4405	0.2105	45.0403	0.6240

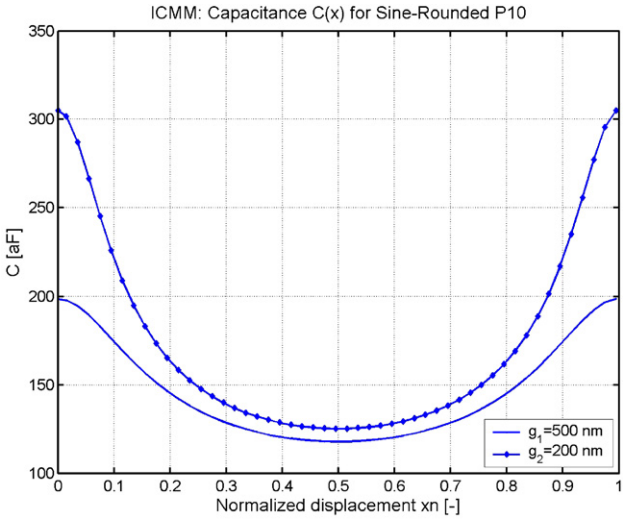

Figure 9. The simulated capacitance function $C(x)$ for two gaps $g_1 = 500$ nm and $g_2 = 200$ nm for the geometry in figure 8 with period size $P_x = 10$ μm.

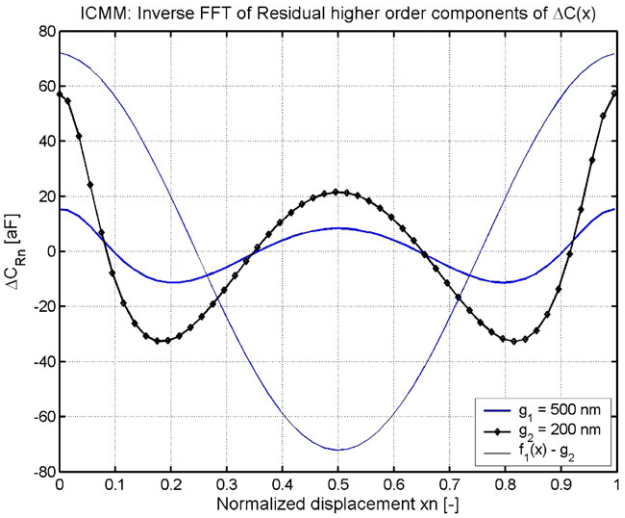

Figure 10. (ICMM) Calculated inverse FFT of all residual higher-order components in the FFT spectrum of the capacitance functions in figure 9. For comparison the first-order harmonic for g_2 is also given.

residual space domain function $r(x_n)$ is on average around 62% of the amplitude of the first harmonic $f_1(x)$.

Figure 10 gives the resulting residual function $r(x)$ for g_1 and g_2. For comparison, the first-order harmonic $f_1(x)$ of the simulated $C(x)$ for a gap $g_2 = 200$ nm is also given.

4.2. Nonlinearity study for CCMM

This section gives the results for the nonlinearity study of CCMM following the same approach as in the previous section

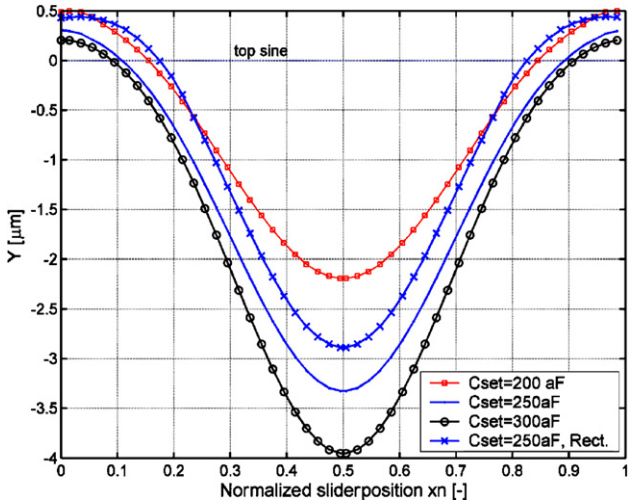

Figure 11. Simulated $y(x)$ for different setpoints C_{setpoint}. The value $y(x = 0)$ is the minimum gap g.

for ICMM. For every displacement of the rounded finger in figure 8 in the x-direction, a displacement in the y-direction is calculated in order to keep the calculated capacitance $C(x, y(x))$ equal to the setpoint C_{setpoint}. If $\mathrm{d}C_e = C(x_i, y_j) - C_{\text{setpoint}}) < 1\%$, position y_j is recorded and a new position x_{i+1} is taken. Apart from rounded fingers, rectangular-shaped fingers are also used for the simulation and comparison.

In figure 11 the displacement in the y-direction of geometry S2 is given for every displacement in the x-direction for which the capacitance equals the setpoint capacitance $C(x, y(x)) = C_{\text{setpoint}}$. The $y = 0$ line crosses the top of the sine geometry S1 in figure 8.

For rectangular fingers, the amplitude of $y(x)$ for a setpoint $C_{\text{setpoint}} = 250$ aF is smaller than that for rounded fingers with the same setpoint. The reason is that the capacitance between rectangular-shaped geometries is larger due to charge accumulation at sharp convex corners and an accompanying higher electric field intensity [27]. Therefore, for the rectangular fingers to reach a certain setpoint capacitance requires a smaller displacement in the y-direction.

Because of the convolution nature of the capacitance between the two geometries, the shape of $y(x)$ for the rectangular finger is less corresponding to a sine than for the rounded finger. This is also clearly reflected in the amplitudes and ratios between the first-order and higher-order harmonics of the simulated curves for $y(x)$, given in table 3. Figure 12 gives the inverse FFT of the residual higher-order components of $y(x)$, i.e. $r(x_n) = \text{IFFT}\ (A(n{\cdot}\omega_0))$ for $n \neq 0, 1$. Also, the fundamental $f_1(x)$ of $y(x)$ is displayed.

Table 3 shows that the amplitudes of the higher-order frequency components in the simulated $y(x)$ function for the geometry with a rounded finger and sine pattern are about 11% of the first-order harmonic, for a setpoint capacitance of $C_{\text{setpoint}} = 300$ aF/period. This is about 62% of that for

Table 3. CCMM amplitudes and ratios for the FFT components of simulated $y(x)$ for different setpoints C_{setpoint}.

C_{setpoint} (aF)	$A_{\omega 0}(x)$ (μm) $_{(\omega 0=0.2\pi)}$	$A_{2\omega 0}/A_{\omega 0}$	$A_{3\omega 0}/A_{\omega 0}(x)$	$\overline{r(x_n)}$ (μm)	$\overline{r(x_n)}/A_{\omega 0}$
200	1.348	0.056	0.0026	0.0829	0.0615
250	1.8186	0.0895	7.12×10^{-4}	0.1616	0.0888
300	2.0919	0.1082	0.0015	0.2310	0.1104
250R	1.7143	0.1435	0.0276	0.2867	0.1576

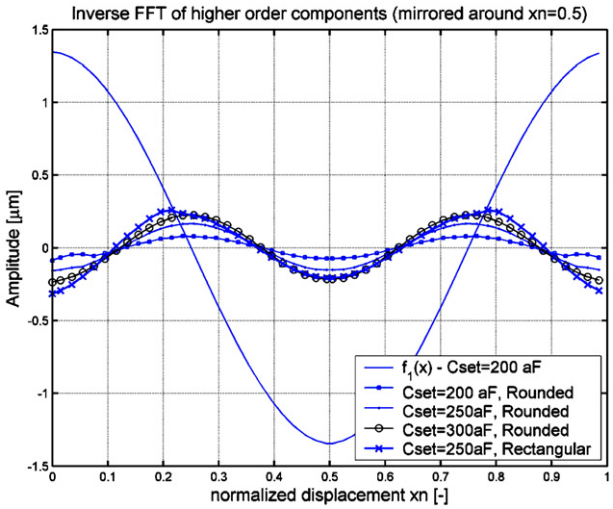

Figure 12. The residual function $r(x_n)$ is the difference between $y(x)$ and a pure sine-function with amplitude $A_{\omega 0}$ and period $P_x = 10$ μm.

ICMM as given in table 2. In other words, for CCMM the nonlinearity is much smaller than that for ICMM, as predicted by the analysis in section 2.3. Therefore, the ideal geometry combination that produces a pure sine-function $C(x)$ for the ICMM concept will not be the same ideal geometry combination that produces a perfect sine-function $y(x)$ for the CCMM concept.

However, for an increase in the setpoint capacitance for CCMM from $C_{\text{setpoint}} = 200$ aF to 300 aF, the ratio of higher-order frequency components and first-order harmonic also increases. This is probably because the ratio of the period size P_x and the width w of the rounded fingers is not exactly a situation with probe-like dimensions as discussed in section 2.3. Taking rounded fingers with a finger length $L_f > 2A$ (figure 2) gives a better result than rectangular fingers.

2D FE simulation results sustain the conclusion of the CCMM analysis in section 2.3 in terms of the expected shape of $y(x)$ for the geometry combination of a sine with a finger-like pattern. The predictions for CCMM in terms of the SNR improvement have not been examined. However, for all calculated positions the capacitance can be $C(x, y(x)) = C_{\text{setpoint}} = 300$ aF while for ICMM the capacitance $C(x) = 300$ aF only around $x = 0$ and $C(x) = 125$ aF around $x = P_x/2$ for the given geometry and ratio of feature sizes. Therefore, regarding the capacitance measurement, the SNR can be higher for CCMM than for ICMM at given noise levels.

5. Conclusions

This paper (part 1) presents an analysis and a simulation for a capacitive incremental position sensor for nanopositioning of microactuator systems.

Two related concepts for a capacitive incremental position sensor are presented. In an incremental capacitance measurement mode (ICMM) the periodic change in capacitance between two periodic geometries S1 and S2 is measured to determine the relative displacement between S1 and S2. In a constant capacitance measurement mode (CCMM) the distance between S1 and S2 is controlled to keep the capacitance between S1 and S2 constant.

A theoretical approximation shows that the signal-to-noise ratio for CCMM can be $>300\times$ over ICMM. A theoretical and 2D finite element method analysis shows that the position sensing signal for CCMM will better approximate a sine than ICMM, if geometry S1 is sine and geometry S2 has rounded fingers with probe-like dimensions. A pure sine position-sensing signal is desired for quadrature incremental position detection with nanometer accuracy over an infinite displacement range. At the expense of more controlled complexity, the CCMM concept is expected to result in a higher position accuracy with less nonlinearity.

A comparison between 2D FE simulations and measurements for ICMM shows that the concept of a periodically changing capacitance can be realized, and the 2D FE simulation method realistically predicts the capacitance versus displacement for different combinations of periodic geometries. Therefore, as an alternative to the computationally more time-consuming 3D FE simulations, the 2D FE method can be used for further analysis and optimization of the two incremental position-sensing concepts.

Acknowledgments

This research is financed by the Dutch Technology Foundation STW. The authors would like to thank M de Boer, E Berenschot, R Sanders, H van Wolferen and the MESA$^+$ laboratory staff for their contribution to the fabrication and measurements.

References

[1] Vettiger P, Desmont M, Drechsler U D, Ürig U H, Äberle W, Luwyche M I, Rothuizen H E, Stutz R, Widmer R and Binnig G K 2000 The 'Millipede'—more than one thousand tips for future AFM data storage *IBM J. Res. Dev.* **44** 323–40

[2] Abelmann L, Bolhuis T, Hoexum A M, Krijnen G J M and Lodder J C 2003 Large capacity probe recording using storage robots *IEE Proc.* A **150** 218–21

[3] Binnig G, Quate C F and Gerber C 1986 Atomic force microscope *Phys. Rev. Lett.* **56** 930

[4] Deladi S, Berenschot J W, de Boer M J, Krijnen G J M and Elwenspoek M C 2004 An AFM-based device for *in-situ* characterization of nano-wear *Proc. MEMS 2004 (Maastricht, The Netherlands)* p 181

[5] Toshiyoshi H *et al* 1999 Fabrication of micromechanical tunneling probes and actuators on a silicon chip *Japan J. Appl. Phys.* **38** 7185–9

[6] Lim G, Minami K, Sugihara M, Uchiyama M and Esashi M 1995 Active catheter with multi-link structure based on silicon micromachining, *Proc. 8th IEEE Workshop Micro Electra Mechanica Systems (Amsterdam, The Netherlands)* p 116
[7] Mastrangelo C H, Burns M A and Burke D T 1998 Microfabricated devices for genetic diagnostics *Proc. IEEE* **86** 1769–87
[8] Muthuswamy J, Salas D and Okandan M 2002 A chronic micropositioning system for neurophysiology *Proc. 2nd Joint EMBS/BMES Conf. (Houston, TX, USA, 23–26 Oct)*
[9] Bergander A 2003 Micropositioners for microscopy applications and microbiology based on piezoelectric actuators *J. Micromechatronics* **2** 65–76
[10] Grade J D 2004 Advanced, vibration resistant, comb-drive actuators for use in a tunable laser source, *Sensors Actuators* A **114** 413–22
[11] Ferreira A, Agnus J, Chaillet N and Breguet J M 2004 A smart microrobot on chip: design, fabrication and control *IEEE/ASME Trans. Mechatronics* **9** 508–19
[12] Elwenspoek M and Wiegerink R J 2000 *Mechanical Microsensors* (Berlin: Springer)) pp 13–21
[13] Pantazi A, Lantz M A, Cherubini G, Pozidis H and Eleftheriou E 2004 A servomechanism for a micro-electromechanical-system-based scanning-probe data storage device *Nanotechnology* **15** S612–21
[14] Eleftheriou E *et al* 2003 Millipede—a MEMS-based scanning-probe data-storage system *IEEE Trans. Magn.* **39** 2
[15] Chu L L and Gianchandani Y B 2003 A micromachined 2D positioner with electrothermal actuation and sub-nanometer capacitive sensing *J. Micromech. Microeng.* **13** 279–85
[16] Baxter L K *et al* 1997 *Capacitive Sensors: Design and Applications* (New York: IEEE)
[17] Kosel P B, Munro G S and Vaughan R 1981 Capacitive transducer for accurate displacement control *IEEE Trans. Instrum. Meas.* **2** 114
[18] Klaassen K B and van Peppen J C L 1982 Linear capacitive microdisplacement transduction using phase read-out *Sensors Actuators* **3** 209–20
[19] www.opticalencoder.com
[20] www.GlobalSpec.com
[21] Fraden J 1996 *Handbook of Modern Sensors, Physics, Designs and Applications* (New York: Spinger)
[22] Kuijpers A A, Krijnen G J M, Wiegerink R J, Lammerink T S J and Elwenspoek M 2004 Capacitive long-range position sensor for microactuators, *Proc. MEMS (Maastricht, The Netherlands)* p 544
[23] Kuijpers A A, Krijnen G J M, Wiegerink R J, Lammerink T S J and Elwenspoek M 2003 Micromachined capacitive long-range displacement sensor, *Proc. Eurosensors XVII (Guimarães, Portugal, 21–24 September)* pp 560–3
[24] Kuijpers A A, Krijnen G J M, Wiegerink R J, Lammerink T S J and Elwenspoek M 2003 2D-finite-element simulations for long-range capacitive position sensor *J. Micromech. Microeng.* **13** S183–9
[25] Kuijpers A A 2004 Micromachined capacitive long-range displacement sensor for nano-positioning of microactuator systems *PhD Thesis* University of Twente, Enschede, The Netherlands
[26] www.femlab.com, comsol, Sweden
[27] Cheng D K 1989 *Field and Wave Electromagnetics* (Reading, MA: Addison-Wesley)